

Predictability of a Coupled Model of ENSO Using Singular Vector Analysis. Part II: Optimal Growth and Forecast Skill

YAN XUE,* M. A. CANE, AND S. E. ZEBIAK

Lamont-Doherty Earth Observatory, Columbia University, Palisades, New York

T. N. PALMER

ECMWF, Shinfield Park, Reading, United Kingdom

(Manuscript received 5 April 1996, in final form 16 December 1996)

ABSTRACT

The fastest perturbation growth (optimal growth) in forecasts of El Niño–Southern Oscillation (ENSO) with the Zebiak and Cane model is analyzed by singular value decomposition of forward tangent models along forecast trajectories in a reduced EOF space. The authors study optimal growth in forecast runs using two different initialization procedures and discuss the relationship between optimal growth and forecast skill.

Consistent with Part I of this work, one dominant growing singular vector is found. Most of the variation of optimal growth, measured by the largest singular value, for warm events and mean condition is seasonal, attributable to the seasonal variations in the background states. For cold events the seasonal optimal growth is substantially suppressed. The first singular vector is approximately white in EOF space, while its final pattern after a 6-month evolution is dominated by the first EOF. The energy norm amplifies between 5- and 24-fold in 6 months. This indicates that small-scale disturbances are able to draw energy efficiently from the mean seasonal background states and evolve into large scales, characteristic of ENSO, in several months.

The difference fields between the initial conditions generated with the standard initialization procedure and the more recent one of Chen et al. (referred to as old and new ICs) are often so large that the optimal growth for the two sets of forecasts is very different. In such situations, linear growth is not an adequate measure of predictability of ENSO. That the present ZC forecast skill is significantly improved by the new initialization procedure indicates that the inherent ENSO predictability is only a secondary factor controlling current forecast skill; the imbalances between the model and data discussed by Chen et al. are the primary factor.

Optimal growth describes dominant initial error growth only when initial error covariance is white under a choice of norm. If the difference fields between the old and new ICs are considered representative of the error fields of the old ICs, the initial error covariance is red under the energy norm. So a new norm that makes the initial error covariance white is used. The first singular vectors under the new norm are insensitive to initial time and optimization time, and are dominated by the first few EOFs. When the first singular vector components of the initial error fields are removed from the old ICs, the forecast skill is improved significantly. Thus the suppression of a single initial error structure accounts for most of the new scheme's improvement in forecast skill.

1. Introduction

The first successful real-time El Niño–Southern Oscillation (ENSO) forecast with a dynamical model was made in early 1986 (Cane et al. 1986) using the Zebiak and Cane (1987) model (ZC hereafter). Since then a variety of numerical models, including coupled GCMs, hybrid coupled models, intermediate coupled models,

and various statistical models have been applied to experimental ENSO forecasting (Latif et al. 1994). Real-time ENSO forecasts are published in the *Experimental Long Lead Forecast Bulletin*, issued quarterly by the Climate Prediction Center of the National Weather Service. Due to the strong changes of atmospheric heating associated with ENSO in the Tropics, the effects of ENSO are felt on global scales. An accurate prediction of ENSO seems to be crucial for seasonal climate forecasts in midlatitudes (Palmer and Anderson 1994). Although reasonable forecast skills in terms of large-scale indices, such as the area-averaged sea surface temperature anomaly, have been achieved at 1–2-yr lead times, more efforts are needed to predict small-scale structures and achieve better skills.

One inevitable question is the predictability of ENSO:

* Current affiliation: National Centers for Environmental Prediction, Camp Springs, Maryland.

Corresponding author address: Dr. Yan Xue, NCEP, Room 807, WWB, 5200 Auth Road, Camp Springs, MD 20746.
E-mail: wd01yx@sun1.wwb.noaa.gov

Are there intrinsic limits on forecast skill? Singular-vector analysis is a tool to address this issue. In Part I (Xue et al. 1997), this tool has been applied to some idealized climatic states: the seasonal background (zero anomaly) and the ENSO cycles in a long model run. With a choice of norm, the singular vectors of a forward tangent model are a series of orthogonal patterns that amplify at the rate given by the corresponding singular values. A forward tangent model is constructed along a control run trajectory in a climatic phase space (Lorenz 1965). Singular vectors and singular values vary with start times and duration times of control run trajectories. Optimal growth, measured by the largest singular value, is realized if random initial errors assume the fastest-growing configuration (the corresponding singular vector). Usually the spread of forecast errors in ensemble forecasts is much smaller than that given by optimal growth. So optimal growth sets the upper limit of error growth and the lower limit of predictability. We found in Part I that the optimal growth varies seasonally due to the seasonal background specified in the model (annual cycle), and for a 6-month duration it is largest for an early spring start and smallest for a fall start (also see Chen et al. 1997; Moore and Kleeman 1996). The singular vectors corresponding to the optimal growth were found to be insensitive to initial climatic states, but the final patterns after a 6-month evolution depend on how the control run trajectories evolve.

Here singular vector analysis is applied to the actual ENSO cycles in forecasts with the Zebiak and Cane (ZC) model. Since the winds of the simple atmospheric model derived from the observed SST are not realistic out of a narrow equatorial band, the oceanic component of the ZC coupled model is traditionally spun up by the Florida State University (FSU) observed winds. Once the atmospheric and oceanic components are coupled together, the ocean state must adjust to the new model winds. This initial adjustment is a major limitation on the model's forecast skill. It will be shown, however, that the optimal growth of singular vectors is sometimes large enough to limit the model's performance as well.

In an idealized situation where the model is accurate, and initial errors are random and evolve linearly, optimal growth represents the fastest initial error growth. Since random initial errors are inevitable, the model forecast skill will be unreliable when optimal growth is large and be reliable when optimal growth is small. In such a situation, the model's performance will mainly be determined by the predictability of the system. However, when initial errors are very large and evolve nonlinearly, linear theory is not valid. The largest singular value, as a measure of local linear error growth rate, may not correspond to the finite-amplitude error growth rate at all. The forecast skill of the ZC model has recently been improved significantly by implementing a new initialization procedure [Chen et al. (1995); henceforth we will refer to the original and improved forecasts as old and new, respectively]. The old and new forecasts

are subjected to singular vector analysis in the present work. We will investigate whether the initial error growth in the ZC forecasts can be described by the linear analysis and whether optimal growth is an indicator of the model's forecast skill as discussed in the above idealized situation.

This paper is organized as follows. Section 2 briefly describes the old and new forecasts with the standard and new initialization procedures, respectively, and the following two sections describe the forward tangent models linearized about the two sets of forecasts for lead times up to 6 months. Using the energy norm, the singular vectors and singular values of the local forward tangent models for each start month between January 1970 and December 1994 for the two sets of forecasts were analyzed, respectively. In section 5, the differences between the largest singular values of the old and new forecasts are discussed. Another set of singular vector analysis using a new norm is carried out in section 6. Under the new norm, the first singular vectors are shown to be the most significant components of the difference fields between the old and new initial conditions (ICs), responsible for most of the improvement of the forecast skill of the new forecasts over that of the old forecasts. Section 7 summarizes the results.

2. Old and new forecasts

Chen et al. (1995) designed a new initialization procedure that incorporates air-sea coupling. In the standard initialization procedure (Cane et al. 1986), the observed FSU winds are used to force the oceanic component of the model starting from January 1964 to the time when the coupled forecast starts. The SST field from the wind-forced oceanic component is used to force the atmospheric component, from which the atmospheric initial conditions are taken. Once the atmospheric and oceanic components are coupled, the system often tends to deviate from the forced uncoupled simulations quickly, a phenomenon referred to as initialization shock (Fig. 1a). The new initialization procedure is designed to reconcile the forced model simulations with the coupled model simulations. In the new initialization procedure the model winds are merged with the observed winds, and the result is used to force the oceanic component. Since the model winds on the equator are considerably better than those off the equator, higher weight is assigned to the model winds near the equator. Using this procedure, the divergence of the forecast states from the forced initial condition states is much less prominent (Fig. 1b). Overall, the SST field of the new ICs correlates better with observations than that of the old. Because of the involvement of the coupled processes in the new initialization, the errors from imbalances between the model and data are significantly reduced and, possibly, some wind data errors are also reduced. As a result, the model's forecast skill is substantially improved (see Chen et al. 1995).

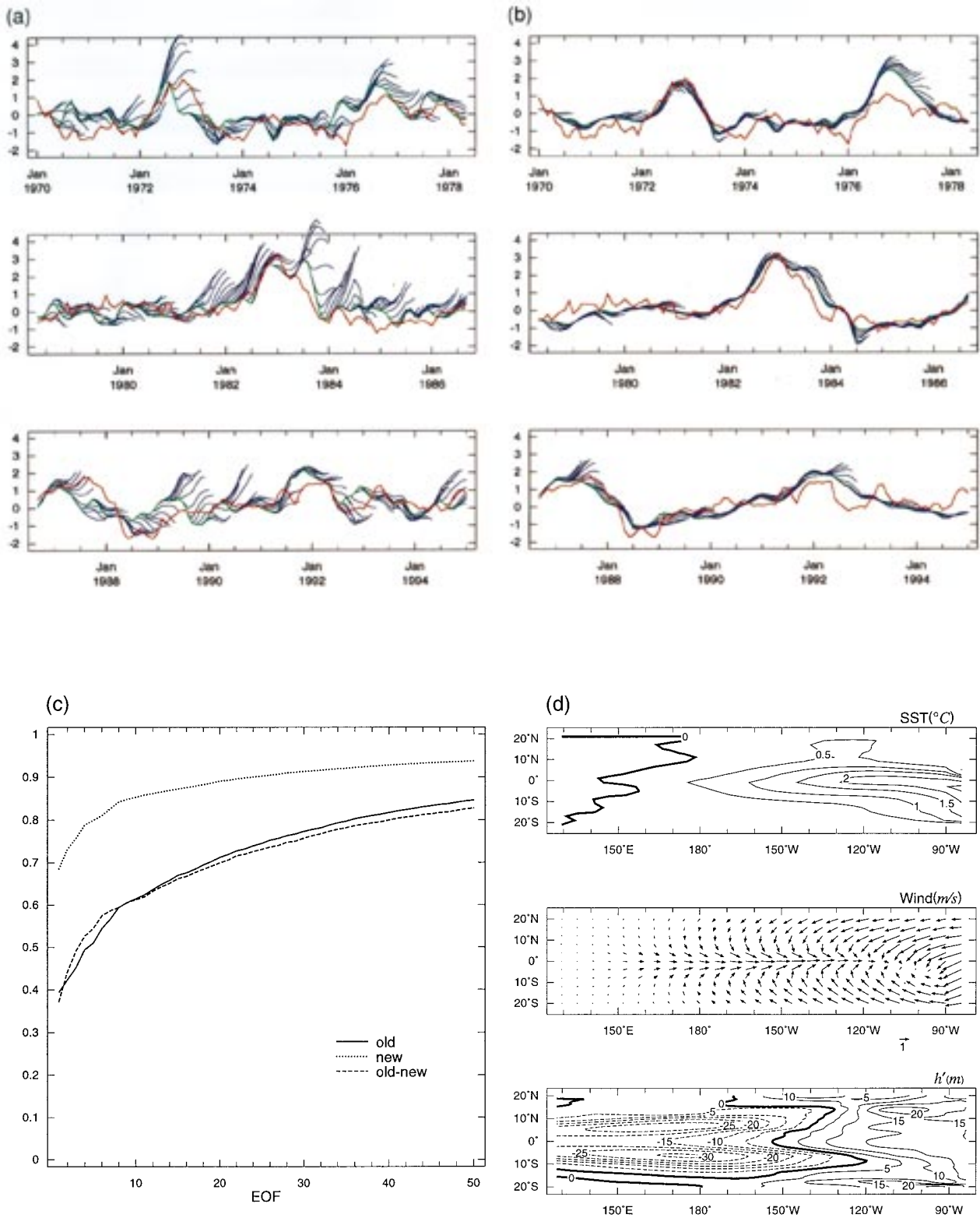


FIG. 1. The Nino-3 indices of the observations (red) and the 6-month forecasts (blue) from (a) the old initial conditions and (b) the new initial conditions as functions of the initial times between January 1970 and December 1994. The forecasts at 0-month lead are labeled green. (c) The cumulative variance distribution of the old initial condition states (solid line), the new initial condition states (dotted line), and the difference fields between the old and new initial conditions (dashed line) among the multivariate EOFs. (d) The first multivariate EOF in the fields of SST, winds, and thermocline depth anomalies.

The initial conditions and predicted states up to 2-yr lead times for the old and new forecasts were projected onto the multivariate EOF structures, which were used to construct the forward tangent models in Part I. Figure 1c shows that the first multivariate EOF accounts for 69% of the variance of the new ICs and only 38% of the variance of the old ICs. This indicates that the new ICs are very much dominated by the first EOF, while the old ICs distribute their energy among many EOFs. The difference fields between the old and new ICs have a similar spectrum to that of the old ICs. The first multivariate EOF takes 37% of the variance of the difference fields. The second and third EOFs account for 7% and 5% of the variance, respectively. The covariance matrix of the difference fields was used to calculate another set of EOFs; the first three EOFs account for 40.5%, 10%, and 5.5% of the variance of the difference fields, respectively. As expected, the first EOF is very similar to that used to construct the forward tangent models and describes the mature phase of ENSO (Fig. 1d). We conclude that the difference fields between the old and new ICs are well described by the 50 EOFs and are dominated by large scales, characteristic of ENSO.

3. Singular vector analysis for the old forecasts

Singular vectors and singular values of forward tangent models are dependent upon norm definition. In this section the L_2 norm in the multivariate EOF space is used, which is also called the energy norm because it is the sum of the variances. The ocean dynamic variables (currents and thermocline depth), SST, and wind anomalies are equally weighted, while the divergence and heating anomalies are weighted much less [Eq. (1) of Part I]. If a matrix \mathbf{L}_τ represents a forward tangent model of τ -month duration, the singular vectors \mathbf{u}_j of \mathbf{L}_τ are the eigenvectors of $\mathbf{L}_\tau^T \mathbf{L}_\tau$,

$$\mathbf{L}_\tau^T \mathbf{L}_\tau \mathbf{u}_j = \sigma_j^2 \mathbf{u}_j, \quad (1)$$

where σ_j are the singular values, representing the amplification factors under the energy norm:

$$\frac{\|\mathbf{L}_\tau \mathbf{u}_j\|}{\|\mathbf{u}_j\|} = \left(\frac{\mathbf{u}_j^T \mathbf{L}_\tau^T \mathbf{L}_\tau \mathbf{u}_j}{\mathbf{u}_j^T \mathbf{u}_j} \right)^{1/2} = \left(\frac{\mathbf{u}_j^T \sigma_j^2 \mathbf{u}_j}{\mathbf{u}_j^T \mathbf{u}_j} \right)^{1/2} = \sigma_j. \quad (2)$$

The singular values are numbered in descending order; hence, the first singular value is the largest singular value.

Relative to the old forecast run trajectories for up to 6-month lead starting from each month between January 1970 and December 1994, monthly forward tangent models were built using Eq. (9) of Part I. As a measure of the degree of linearity, we note that the first singular values of the monthly transition matrices built with positive and negative perturbations (0.1% of the total variance of the initial states) are generally in good agreement (differences are less than 5%). The average of the two monthly transition matrices built with positive and

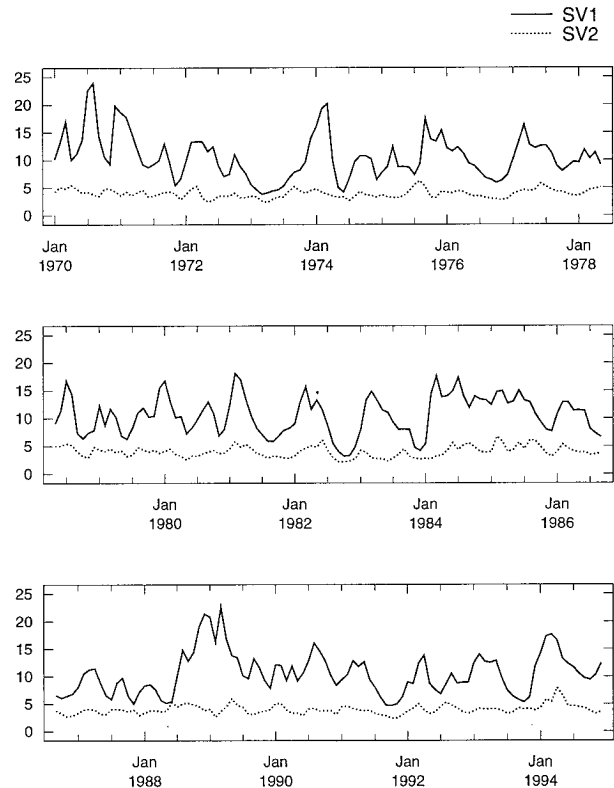


FIG. 2. The first (solid line) and second (dotted line) singular values of the local forward tangent models optimized at 6 months under the energy norm as functions of the old initial condition states.

negative perturbations is taken as the monthly forward tangent model. The forward tangent model for a 6-month transition is the product of six monthly forward tangent models. Figure 2 shows that the first singular value optimized at 6 months is often much larger than the second singular value, and they are comparable when both of them are small. Subsequently we will discuss only the first singular values.

For verification of the forward tangent models, the first singular vector of each local forward tangent model optimized at 6 months with positive and negative signs used to perturb each initial state, from which two perturbed nonlinear model runs are carried out. The differences between the perturbed nonlinear model runs and the control run are called perturbations. The initial amplitude of the perturbations is equal to that of the pattern shown in Fig. 3a of Part I; its maximum amplitudes of SST, wind, and sea level anomalies are approximately 0.1°C , 0.1 m s^{-1} , and 0.6 cm , respectively. The absolute Nino-3 and Nino-4 indices [defined as the averaged SST in the areas of $(5^\circ\text{N}-5^\circ\text{S}, 150^\circ-90^\circ\text{W})$ and $(5^\circ\text{N}-5^\circ\text{S}, 160^\circ\text{E}-150^\circ\text{W})$, respectively) of the perturbations in the two perturbed nonlinear model runs at 6-month lead are compared with the Nino-3 and Nino-4 indices of the perturbations evolved by the forward tangent models (Fig. 3). It is seen that the model is ap-

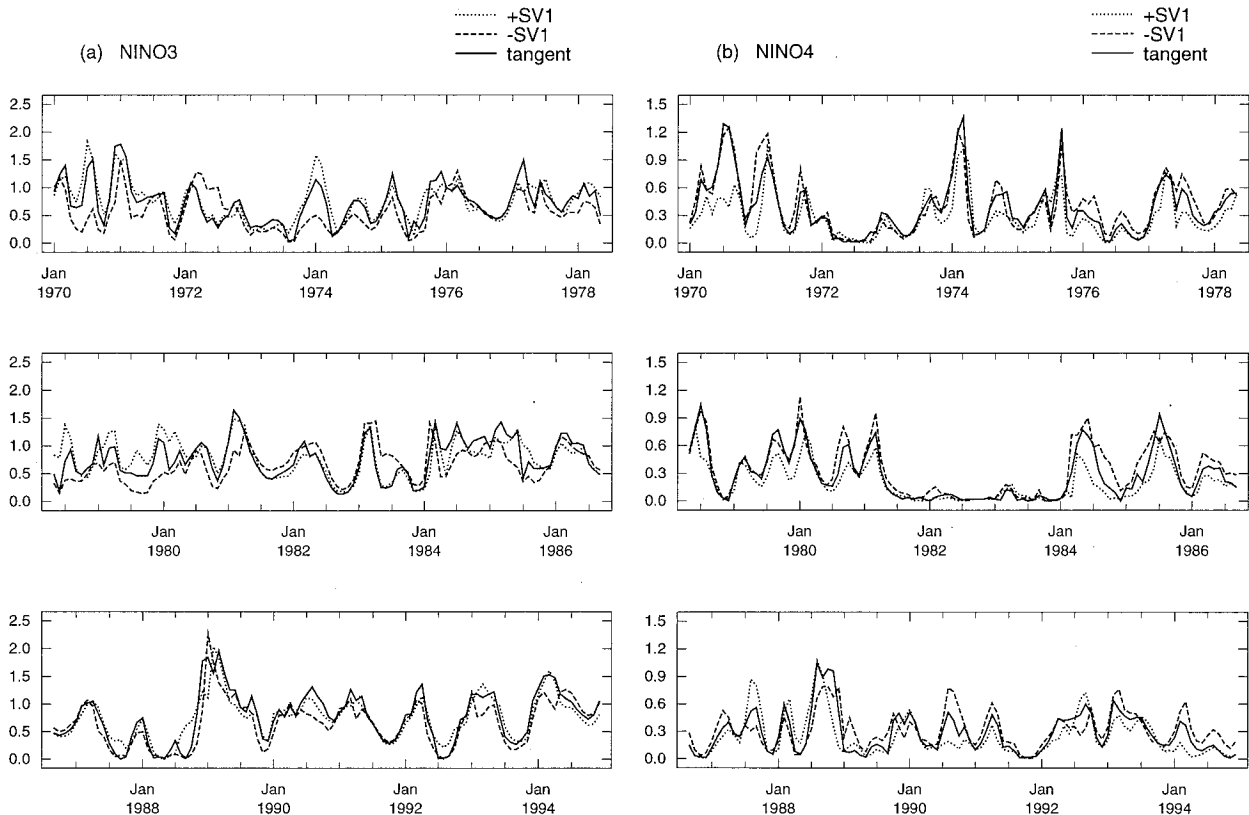


FIG. 3. Comparison of the (a) absolute Nino-3 and (b) Nino-4 indices of the perturbations at 6-month lead in the two perturbed nonlinear model runs initiated from positive (dotted line) and negative (dashed line) first singular vector perturbations of the local forward tangent models for the old initial conditions optimized at 6 months, and that evolved by the forward tangent models (solid line).

proximately linear for 6 months. The prominent nonlinear periods are around June 1970, January 1974, and July 1978 and 1979. It is found that during those periods the initial conditions are close to the climatological mean state (zero anomaly), and with positive and negative first singular vector perturbations the model's thermocline depth in the eastern Pacific evolves into positive and negative anomalous states, respectively, in 6 months. The discontinuity of the subsurface temperature slope at zero thermocline depth anomaly introduces strong nonlinearity (Fig. 1 of Part I). This nonlinearity can be further enhanced by the nonlinear advection term in the SST equation. For example, in September 1988 the negative singular vector perturbation propagates all the way to the western boundary, while the positive singular vector perturbation is confined to the eastern Pacific and grows into a larger amplitude (not shown). This is because the nonlinear advection tends to promote positive perturbations and diminish negative perturbations in the eastern Pacific while inhibiting positive perturbations from moving to the western Pacific and aiding the westward propagation of negative perturbations (Fig. 6 of Part I). The periods surrounding May 1972 and May 1983 have a different kind of nonlinearity where the negative perturbations grow faster than the positive perturbations (Fig. 3a). Based on the fact that

the model generates unrealistic large anomalies in 6 months starting from these initial conditions (Fig. 1a) and the final patterns of perturbations have localized and very fine structures (not shown), we suspect that the nonlinear advection is the primary factor in producing this kind of nonlinearity.

The first singular vectors are found to be insensitive to both initial time and optimization time, which is consistent with the results in Part I. The first singular vectors optimized at 3 months are only slightly suboptimal for 6-month growth, compared to the first singular vectors optimized at 6 months (Fig. 4). Also, the average of the 12 singular vectors of the forward tangent models about the seasonal background starting from each calendar month optimized at 6 months (Fig. 3a of Part I) grows almost as fast as the 6-month optimal singular vectors (Fig. 4). Although the first singular vectors are very similar, their final patterns are strong functions of the initial states. The variability of the final patterns of the first singular vectors in the eastern and western Pacific, measured by Nino-3 and Nino-4 indices, is clearly seen in Fig. 5. For the ENSO cycles in a long model run we showed in Part I that during the warm phases of ENSO the growth in Nino-3 is generally much larger than the growth in Nino-4; in contrast, during the cold phases of ENSO the growth in Nino-3 and Nino-4 are com-

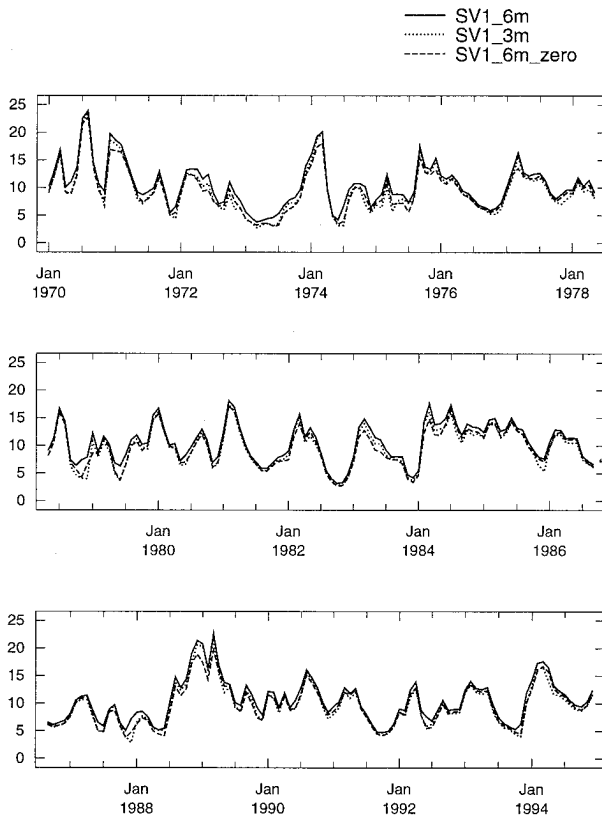


FIG. 4. Comparison between the optimal 6-month growth rates (solid line), the 6-month growth rates of the first singular vectors optimized at 3 months (dotted line), and the 6-month growth rates of the singular vector shown in Fig. 3a of Part I (dashed line) as functions of the old initial condition states.

parable. Similar characteristics of growth rate are found here. Large growth rates in NINO3 and small growth rates in Nino-4 are observed for the five warm events (1972/73, 1976/77, 1982/83, 1986/87, and 1991/92). The growth rate is modulated strongly by season, and for a 6-month optimization it is largest at an early spring start and smallest at a fall start. The growth rate during the non-ENSO periods, for example, the years 1981, 1984, 1985, 1989, 1990, and 1994 (Fig. 1a), can be as large as that during the warm events. During those initial times, the model had ENSO false alarms (Fig. 1a). Generally speaking, when a false warming is forecast from spring, the growth rate can be as large as that during the onset of a true ENSO event. In addition, when the initial conditions are close to the climatological mean (zero anomaly), positive singular vector perturbations often grow much faster than negative singular-vector perturbations, and the final patterns extend to the western Pacific, for example, during the years 1970, 1974, 1978, 1979, 1980, and 1988 (Figs. 1a, 3a, and 5). During the cold phases of ENSO, growth rate is generally small, for example, during the years of 1973 and 1988, which are the only two cold events that the model has simulated under the standard initialization (Fig. 1a); in con-

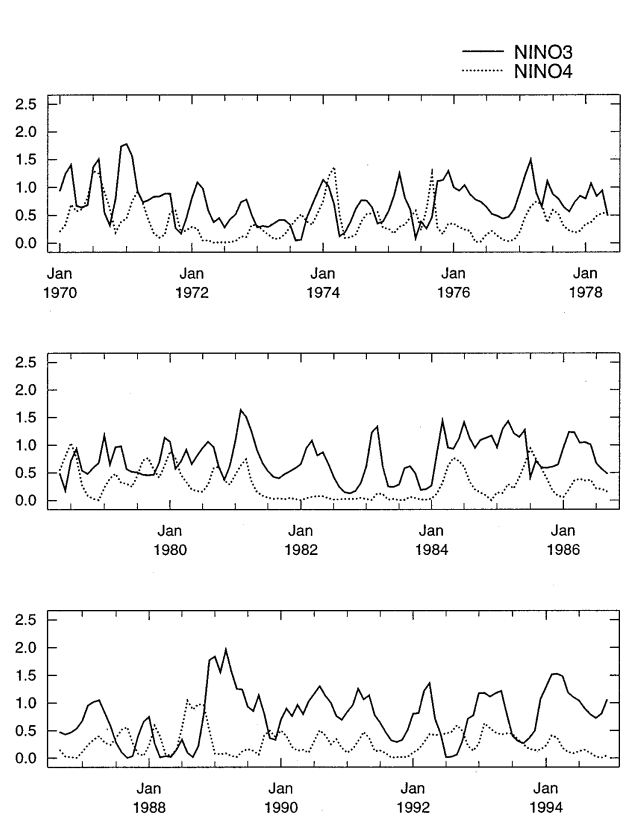


FIG. 5. The Nino-3 (solid line) and Nino-4 (dotted line) indices of the final patterns of the first singular vectors of the local forward tangent models optimized at 6 months as functions of the old initial condition states.

trast to the warm phases in which the final patterns of the first singular vectors are confined to the eastern Pacific, they span both the eastern and the western Pacific at 6-month leads (Fig. 5).

When optimal growth is large, the system is sensitive to perturbations, and forecasts are likely to be unreliable. The amplitude of forecast errors in the direction of the dominant singular vectors depends on the projection of analysis error on that direction at initial time. If the model is accurate, the smaller the growth rate is and the better the forecasts are; while when the growth rate is large, the forecasts can be either good or bad depending on the projection of analysis error on the dominant singular vectors. Since forecast errors vary between zero and a maximum set by optimal growth, the scatter between the forecast errors and optimal growth is expected to form an approximately triangular shape. This is shown in Fig. 6. The months of 1983 are outliers, suggesting that the large forecast errors during that period are not related to large dominant singular vector growth. We note that the model tries to end the 1982/83 event differently from the real system, with easterly wind anomalies in the eastern Pacific instead of in the western Pacific. For the model to perform well, the initial conditions have to be adjusted toward what the model likes.

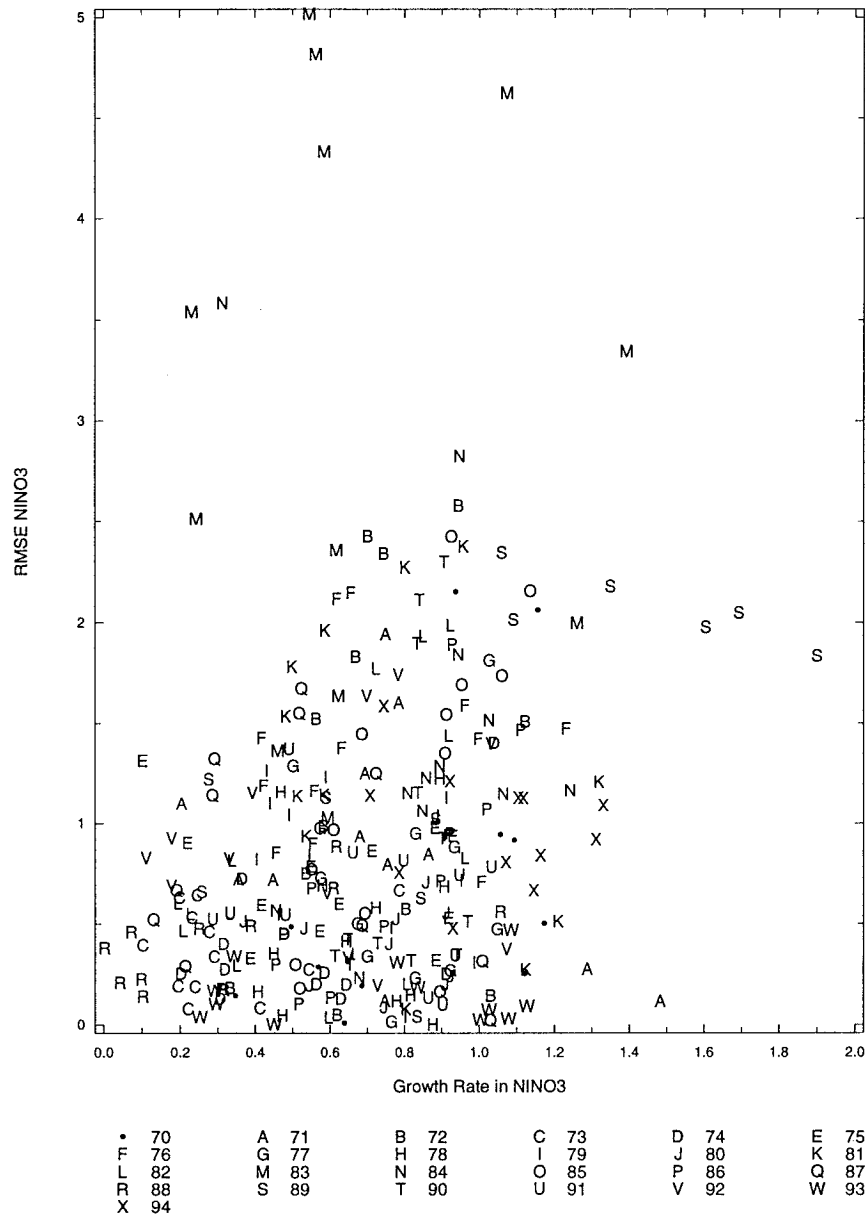


FIG. 6. Scatterplot between the forecast errors in Nino-3 at 6-month lead and the 6-month optimal growth rate in Nino-3 for the old initial conditions. Each year is labeled as a letter.

This is realized by primarily using the model winds near the equator to spin up the oceanic component in the new initialization procedure (Fig. 1b). Another feature in Fig. 6 is that the false ENSO alarms that the model has made in the past two decades are all associated with medium to large growth rates, for example, the years of 1971, 1972, 1976, 1981, 1982, 1984, 1985, 1989, and 1990 (Fig. 1a). During those times the forecast errors in Nino-3 at 6-month lead exceed 1.7°C, and they must have been to some degree attributable to the large growth rates of the system.

In numerical weather prediction, the fastest-growing singular vectors contain mostly small-scale structures,

which evolve into large scales and amplify strongly in 2–3 days (Buizza and Palmer 1995). This poses a serious problem because poorly observed subsynoptic-scale disturbances may be crucial to the development of synoptic-scale circulations. Figure 7 shows the energy distribution among the 50 EOFs of the averaged first singular vector and its final pattern after a 6-month evolution for the old forecasts. The energy of the first singular vector is spread among many EOFs, especially the 2d, 3d, 17th, 18th, and 34th EOFs, while the energy of the final pattern is mostly in the first EOF. This means that an initial small error in the high EOFs can evolve into an ENSO-like pattern in 6 months. Moreover, this

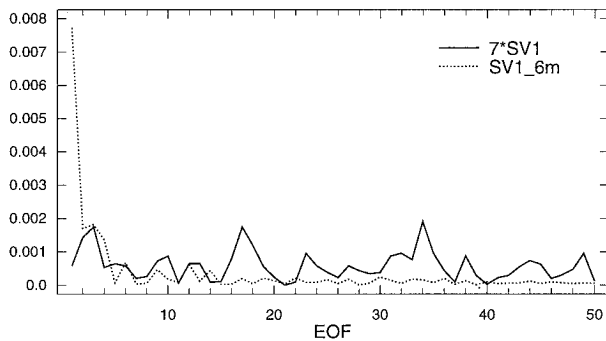


FIG. 7. Energy distribution of the average of the first singular vectors of the local forward tangent models for the old initial conditions optimized at 6 months (times 7, solid line) and their final patterns (dotted line) after a 6-month evolution.

fast error growth is not the primary limitation on the present ENSO forecasts because the initial errors are often in large scales (Fig. 1c). We will discuss this issue further in section 6.

4. Singular vector analysis for the new forecasts

The analysis of the last section was repeated for the new forecasts of Chen et al. (1995). Forward tangent models relative to the forecast trajectories for up to a 6-month lead were constructed. As before, the second singular value is often much smaller than the first singular value (Fig. 8), and the forward tangent models simulate the first singular vector perturbation growth in the nonlinear model very well (Fig. 9). The model is largely in the linear regime, and when it is not [when the two Nino-3 (Nino-4) indices of positive and negative perturbations differ appreciably], the index evolved by the forward tangent model falls between the two nonlinear model cases.

As before, the first singular vectors are not sensitive to initial time and optimization time (Fig. 10), but the final pattern of the first singular vector after a 6-month evolution is a strong function of the initial times (Fig. 11). The dependence of the growth rate on the phases of ENSO is consistent with what we found for the old forecasts (Fig. 5). For the five warm events of 1972/73, 1976/77, 1982/83, 1986/87, and 1991/92, the growth rate in Nino-3 is large while the growth rate in Nino-4 is small. The seasonal modulation of the growth rate is prominent during the warm events. During the non-ENSO years, for example, 1971, 1975, 1979, and 1980, the growth rate is large and is associated with strong nonlinearity (Fig. 9a). During those times the initial conditions are close to the climatological mean state (zero anomaly), so positive perturbations grow faster than negative perturbations (Fig. 1 of Part I). During the four cold events that the model simulated (in 1973, 1978, 1984/85, and 1988/89), the growth rate is small, and the Nino-3 and Nino-4 indices are comparable (Figs. 1b and 11).

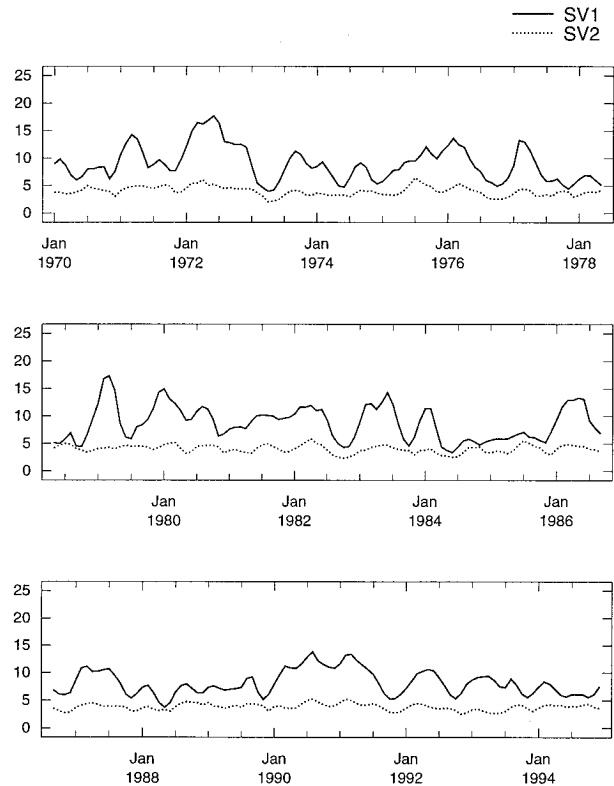


FIG. 8. As Fig. 2 except for the new initial conditions.

The scatter between the forecast errors at 6-month lead and the 6-month optimal growth is shown in Fig. 12. The forecast errors are generally smaller than those of the old forecasts, and the outliers of the months of 1983 and the cluster of the false alarms are gone. Big forecast errors fall mainly in the years of 1976, 1977, 1983, and 1992, and are not necessarily associated with a large growth rate since the initial errors are already very large (Fig. 1b).

5. Comparison of optimal growth

Previously it was mentioned that when the initial conditions are close to the climatological mean, positive singular vector perturbations often grow much faster than negative singular vector perturbations. An averaged growth rate is defined as the average of the absolute Nino-3 indices of positive and negative perturbations. The averaged growth rate for the old and new forecasts is compared to that of the seasonal background in Fig. 13a. The optimal growth rate of the two sets of forecasts is largely consistent with that due to the seasonal background alone, although the seasonal growth rate is occasionally either enhanced or suppressed by interannual variability. For example, the seasonal growth rate due to the seasonal background alone is greatly suppressed during the two cold events of 1973 and 1988, which are simulated in the two sets of forecasts consistently,

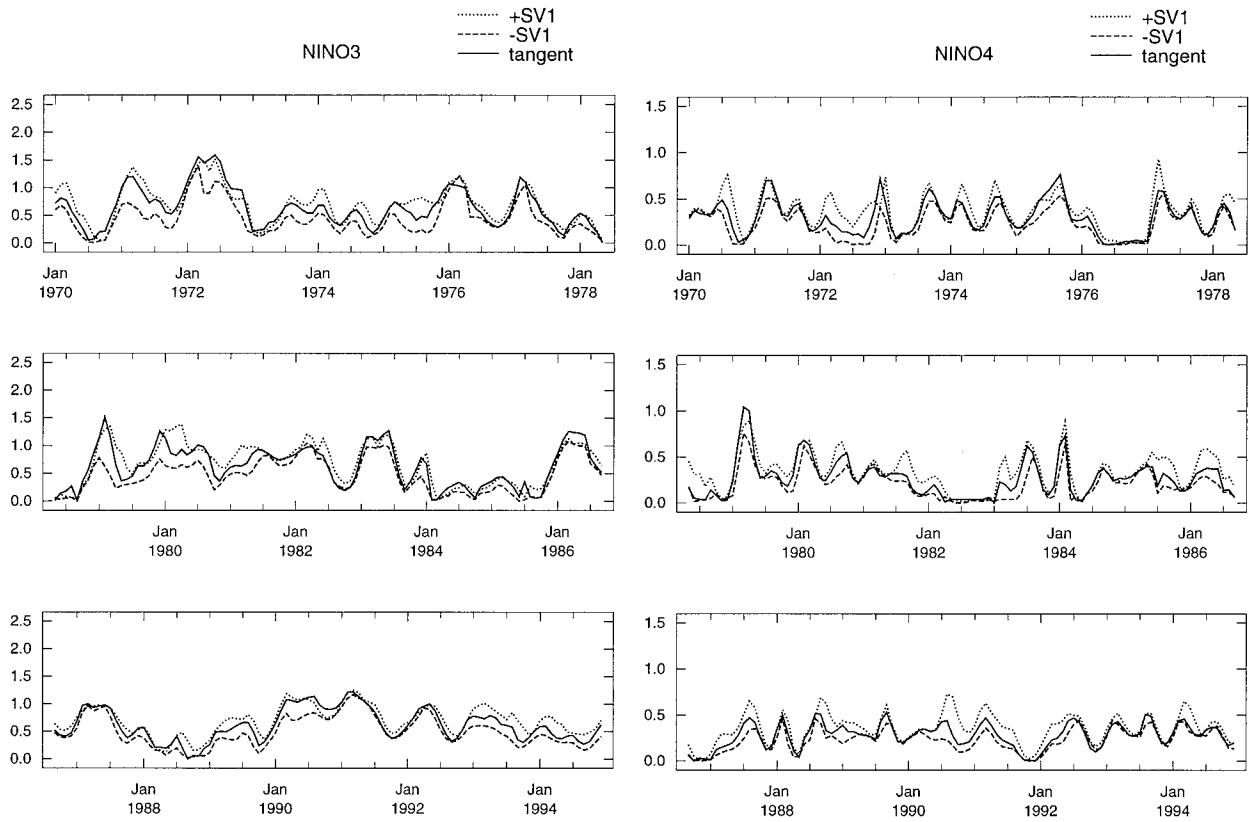


FIG. 9. As Fig. 3 except for the new initial conditions.

and it is greatly enhanced during the non-ENSO years of 1989 and 1994 for the old forecasts. Compared to the growth rate of the old forecasts, the growth rate of the new forecasts is smaller on average (Fig. 13b). This is largely due to the simulation of two more cold events, those of 1978 and 1984/85: the cold events are more stable since the system is less sensitive to thermocline depth perturbations (Fig. 1 of Part I). Also, in late 1970 and 1994 the system is in a weak cold phase instead of a weak warm phase, which results in a smaller growth rate. In the years of 1970, 1978, 1984, 1985, 1989, and 1994, the growth rate changes significantly between the old and new forecasts, which indicates changes of dynamic regimes.

Since the new forecasts simulate the real ENSO system significantly better than the old forecasts, the differences between the old and new ICs can be considered as representative of the errors of the old ICs (at least with respect to the forecast model we are using). During the years when the errors of the old ICs are so large that the old forecasts are wrong, then the optimal growth of the old forecasts fails to represent the predictability of ENSO. In such situations, the ENSO forecast skill is limited more by the initial error fields rather than by the inherent predictability. This is in contrast to the typical case in numerical weather prediction, in which the initial errors have been controlled by sophisticated

data analysis schemes to be so small that the singular-vector growth is usually the principal source of error. Molteni and Palmer (1993) pointed out that the largest singular value is a measure of finite-time predictability, and when it is extremely large, a warning should be issued along with a forecast. In addition, the fastest-growing singular vectors are being implemented into ensemble prediction to obtain a consensus forecast (Molteni et al. 1996). That the ZC forecast skill is far less limited by predictability than by the large initial error fields is hopeful: we have room for improvement before the limits of predictability constrain us.

In Fig. 13b the monthly average of the growth rate for the old and new forecasts and the ENSO cycles in a long model run (Fig. 10c of Part I) are compared to the growth rate about the seasonal background. The growth rate of the old forecasts is very close to the growth rate of the seasonal background, except that the drop of the growth rate from March starts to May starts is sharper, indicating a stronger seasonality. The growth rate of the new forecasts is appreciably less than that of the old forecasts at early spring starts. Therefore the drop of growth rate from March starts to May starts is significantly smaller. This is consistent with the fact that the new forecasts do not seem to experience the spring predictability barrier (Chen et al. 1995). Xue et al. (1994) pointed out that both mean square errors and the

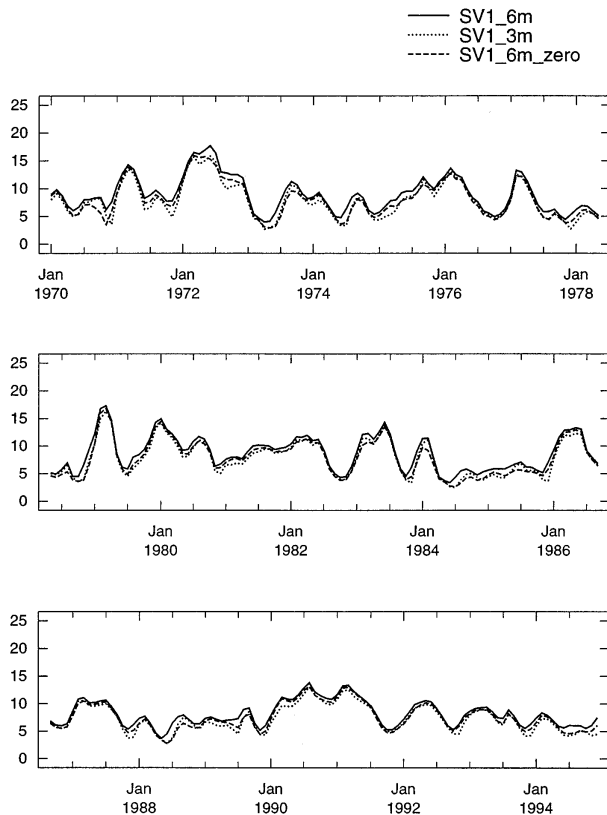


FIG. 10. As Fig. 4 except for the new initial conditions.

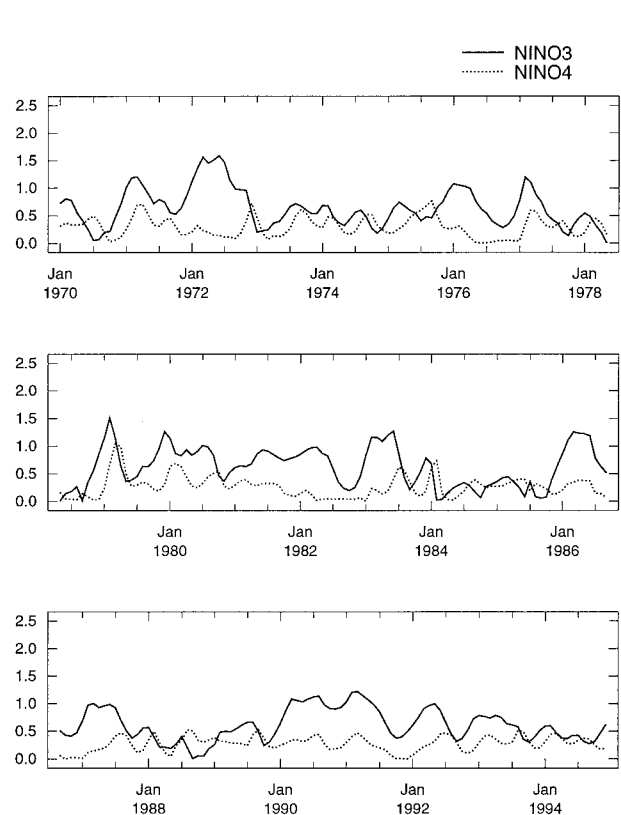


FIG. 11. As Fig. 5 except for the new initial conditions.

smallest signal variance in spring contribute to the spring predictability barrier. Because the initial errors of the old forecasts are quite large and grow fast in the spring and summer seasons, the forecast errors passing through spring at more than a 9-month lead are high enough to degrade the correlation skill dramatically. In contrast, the initial errors of the new forecasts are smaller and grow more slowly in the spring and summer seasons, so the forecast errors passing through spring at more than a 9-month lead are still relatively small and the correlation skills are only slightly lowered by the smallest signal variance in spring. The so-called spring barrier can be overcome by reducing the model forecast errors.

It is interesting to note that the growth rate of the coupled model states in a long model run studied in Part I is significantly smaller than that of the old and new IC states, in which the observational information is included (Fig. 13b). The growth rate of the ENSO cycles in a long model run represents the typical growth rate of the coupled model system. The standard initialization adds to it considerably, while the new initialization scheme has a far better balance between using the observations and not greatly increasing the growth rate of the system. Nonetheless, this result points to the need for still better assimilation methodologies.

It was suggested above that the difference fields be-

tween the old and new ICs represent the error fields of the old ICs. The question is whether the error fields resemble the first singular vector structure. By carefully scanning the error fields, we found two periods where the errors resemble the first singular vector structure and have amplitudes well within the observational errors (Figs. 14a and 15a). Such small initial errors evolve into errors with a size of medium to large ENSO events in 6 months (Figs. 14b and 15b). During such periods the predictability of the system is the main factor controlling the forecast skill. The result suggests that the ENSO forecasts using the ZC model initiated from March 1972 and August 1981 are not reliable. However, the initial errors are often much larger and are dominated by large-scale structures. For example, the initial errors after the peaks of the 1972/73, 1982/83, and 1986/87 events are large (Fig. 1a), so the old and new forecasts behave very differently at these times.

6. Singular vector analysis under a new norm

Although the initial errors are sometimes very large and evolve nonlinearly, the fastest-growing singular vectors from the linear theory of singular vector analysis may represent the components of the initial errors, which dominate the forecast error growth. The norm for singular vector analysis should be chosen such that ini-

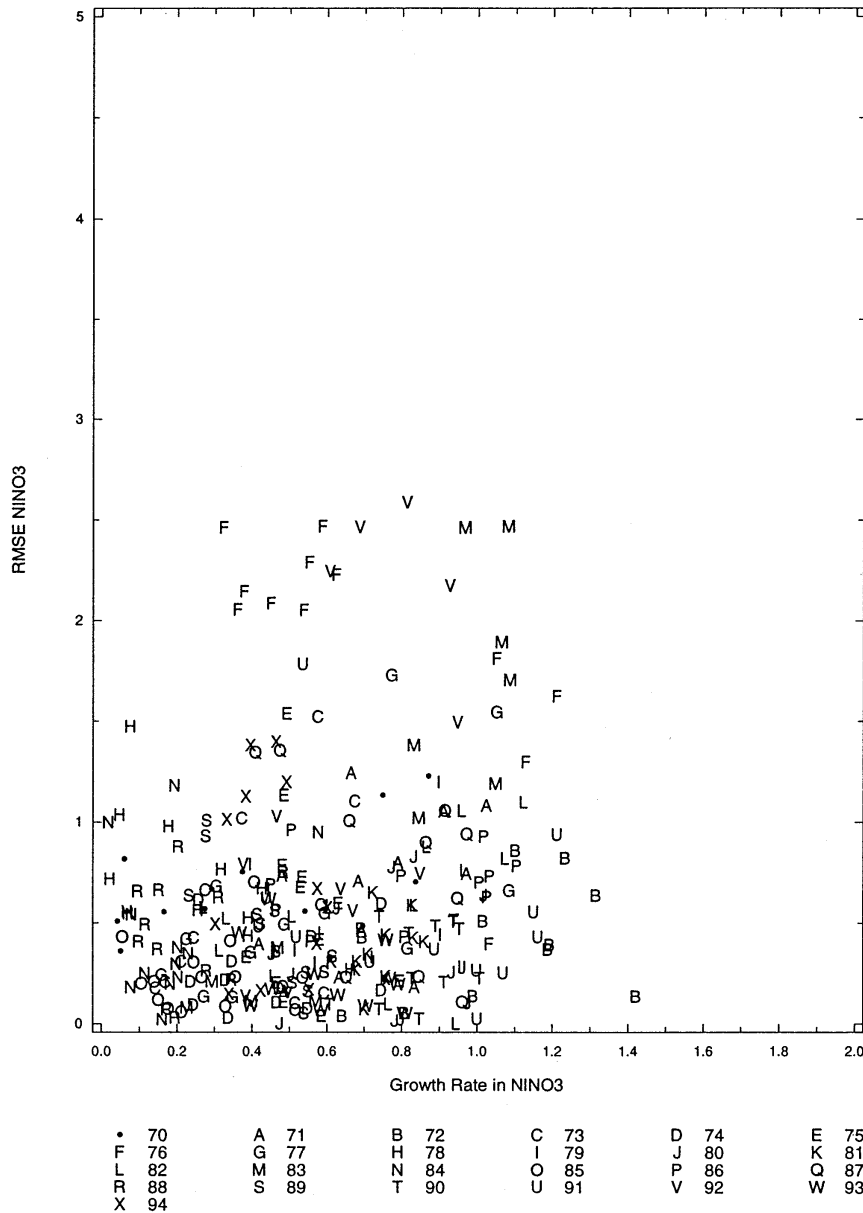


FIG. 12. As Fig. 6 except for the new initial conditions.

tial error covariance is white (the identity matrix) (Palmer 1996). Then the likelihood of the initial errors having the structure of any singular vectors are equal, so the component of the fastest-growing singular vector of the initial errors will contribute the most to the forecast error growth. Under the energy norm used in above sections, the initial errors, the differences between the old and new ICs, are red (Fig. 1c). The initial errors are distributed primarily in the first few EOFs.

Once the initial error covariance is known, it can be used to define a norm under which the initial error covariance becomes the identity matrix. Suppose \mathbf{e}_0 is an initial error vector and \mathbf{C} is the initial error covariance, then $\langle \mathbf{e}_0 \mathbf{e}_0^T \rangle = \mathbf{C}$, where the angle brackets denote an

average over the samples. If \mathbf{C} is decomposed by $\mathbf{C} = \mathbf{U}\mathbf{U}^T$, and a new initial error vector $\mathbf{f}_0 = \mathbf{U}^{-1}\mathbf{e}_0$ is defined, the new initial error covariance $\langle \mathbf{f}_0 \mathbf{f}_0^T \rangle$ is the identity matrix. The error covariance after the evolution by a forward tangent model \mathbf{L} is $\langle \mathbf{e}\mathbf{e}^T \rangle = \langle \mathbf{L}\mathbf{e}_0 \mathbf{e}_0^T \mathbf{L}^T \rangle = \mathbf{L}\mathbf{C}\mathbf{L}^T$. The eigenvectors \mathbf{e}_j of $\langle \mathbf{e}\mathbf{e}^T \rangle$ are the axes of the error ellipsoid, and the root of the eigenvalues, λ_j , are the lengths of the axes. The longest axis represents the largest error. If $\mathbf{e}_j = \mathbf{L}\mathbf{e}_{j0} = \mathbf{L}\mathbf{U}\mathbf{f}_{j0}$, then the eigenvalue problem is

$$(\mathbf{L}\mathbf{C}\mathbf{L}^T)(\mathbf{L}\mathbf{U}\mathbf{f}_{j0}) = \lambda_j^2(\mathbf{L}\mathbf{U}\mathbf{f}_{j0}), \quad (3)$$

or

$$(\mathbf{U}^T\mathbf{L}^T\mathbf{L}\mathbf{U})\mathbf{f}_{j0} = \lambda_j^2\mathbf{f}_{j0}. \quad (4)$$

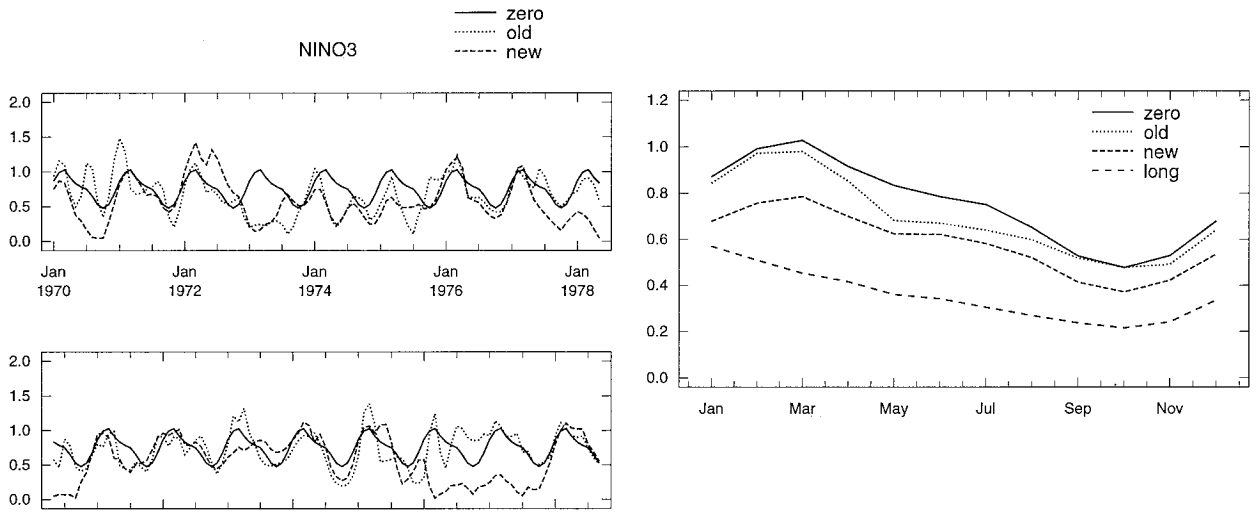


FIG. 13. Comparison between (a) the average of the absolute Nino-3 indices of the perturbations in the two perturbed nonlinear model runs initiated from positive and negative first singular vector perturbations for the seasonal background, repeated every year (solid line), for the old initial conditions (dotted line) and for the new initial conditions (dashed line) as functions of the initial times. (b) The monthly average of the indices shown in (a) plus that for the ENSO cycles in a 12-yr simulation of a long model run (Fig. 10c of Part I).

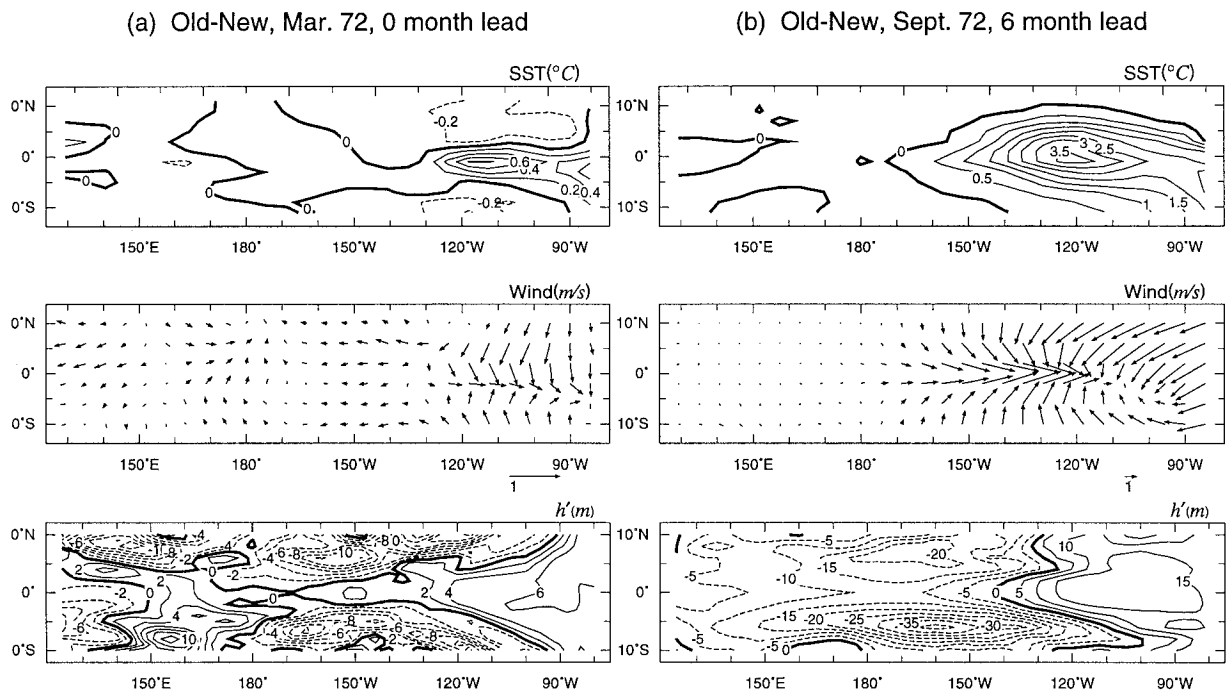


FIG. 14. (a) The difference fields between the old and new initial conditions in March 1972, and (b) the difference fields at 6-month lead.

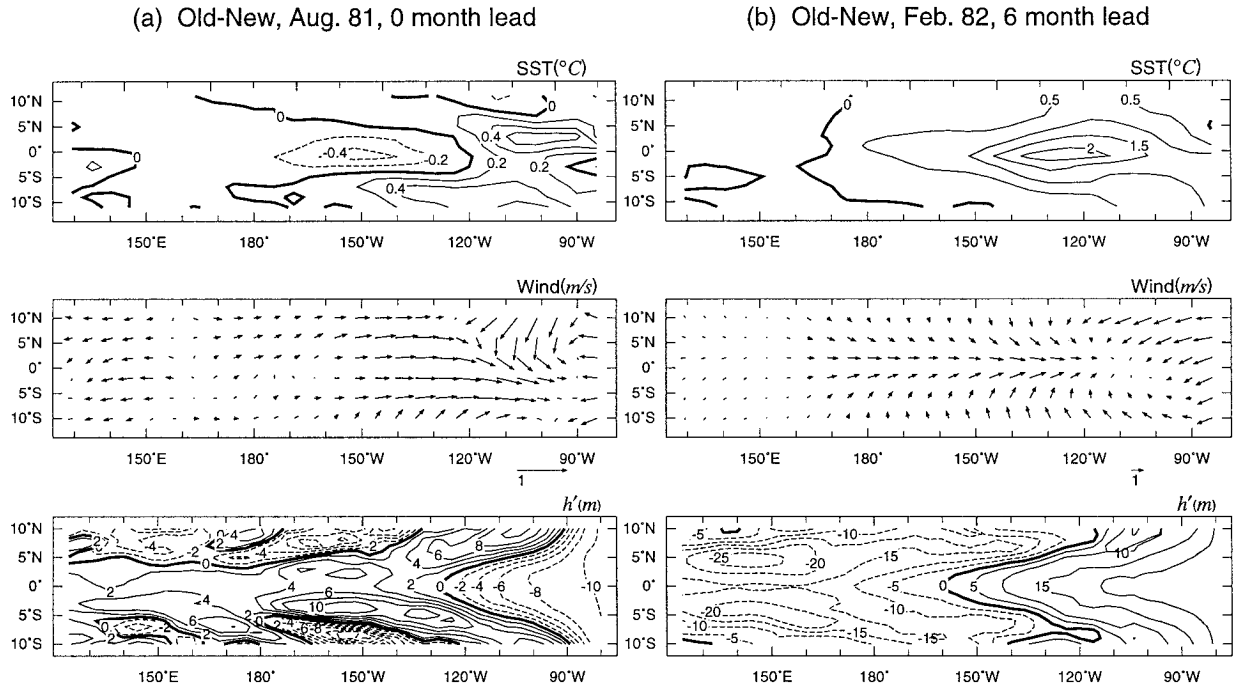


FIG. 15. Same as Fig. 14 except for August 1981.

Here, λ_j is the singular value, and \mathbf{f}_{j0} is the corresponding singular vector; λ_j also describes the ratio of the energy norm of \mathbf{e}_j and the new norm of \mathbf{e}_{j0} , an inner product weighted by \mathbf{C}^{-1} :

$$\begin{aligned} \frac{\|\mathbf{e}_j\|}{\|\mathbf{e}_{j0}\|_{\mathbf{C}^{-1}}} &= \left(\frac{\mathbf{e}_j^T \mathbf{e}_j}{\mathbf{e}_{j0}^T \mathbf{C}^{-1} \mathbf{e}_{j0}} \right)^{1/2} = \left(\frac{\mathbf{e}_{j0}^T \mathbf{L}^T \mathbf{L} \mathbf{e}_{j0}}{\mathbf{e}_{j0}^T (\mathbf{U}^T)^{-1} \mathbf{U}^{-1} \mathbf{e}_{j0}} \right)^{1/2} \\ &= \left(\frac{\mathbf{f}_{j0}^T (\mathbf{U}^T \mathbf{L}^T \mathbf{L} \mathbf{U}) \mathbf{f}_{j0}}{\mathbf{f}_{j0}^T \mathbf{f}_{j0}} \right)^{1/2} = \lambda_j. \end{aligned} \quad (5)$$

Note that λ_j increases with \mathbf{U} ; its absolute value is meaningless. However, the growth rate, defined as the ratio between the energy norm of \mathbf{e}_j and \mathbf{e}_{j0} , is independent of the absolute amplitude of \mathbf{U} because $\mathbf{e}_j = \mathbf{L} \mathbf{e}_{j0} = \mathbf{L} \mathbf{U} \mathbf{f}_{j0}$ and the singular vectors \mathbf{f}_{j0} do not vary with the amplitude of \mathbf{U} . This growth rate must be less than or equal to that in the above sections because the latter is the optimal growth rate under the energy norm.

The difference fields between the old and new ICs for each month between January 1970 and December 1994 are used to calculate the initial error covariance \mathbf{C} . Under the new norm defined above the singular vectors and singular values of each local forward tangent model optimized at 6 months are calculated for the old forecasts. As before, the first singular value is often much larger than the others (not shown). The growth rate of the first and second singular vectors, measured by the ratio of the energy norm of \mathbf{e}_j and \mathbf{e}_{j0} , is shown in Fig. 16. As expected, the growth rate of the first singular vector under the new norm is much smaller than the optimal growth rate (Fig. 2). Note that the

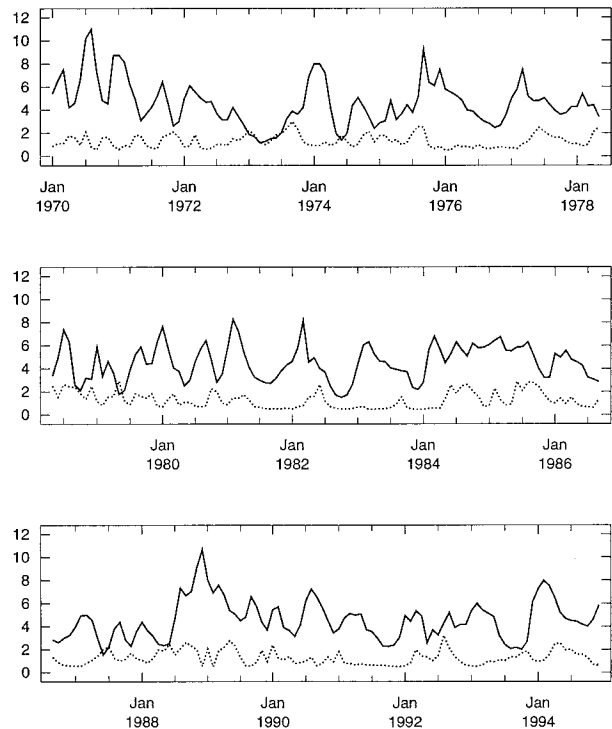


FIG. 16. The 6-month growth rate of the first (solid line) and second (dotted line) singular vectors under the new norm (refer to the text). The growth rate is measured by the ratio of the energy norm of the final and initial perturbations.

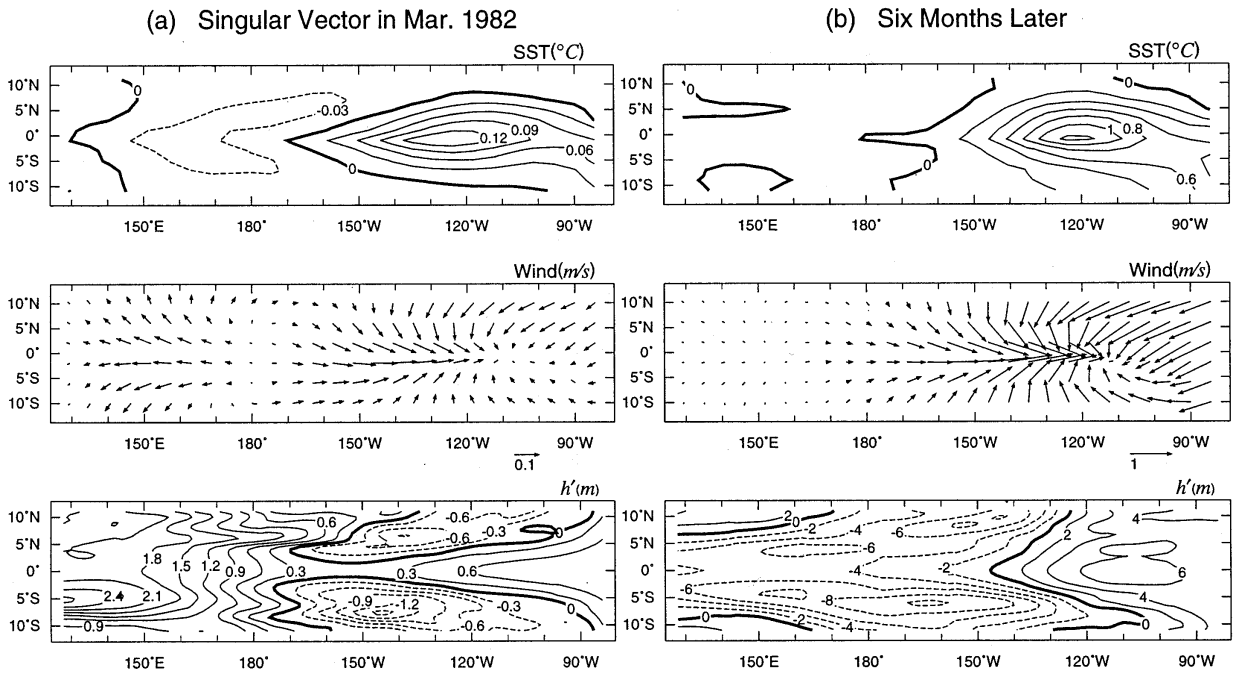


FIG. 17. (a) The first singular vector of the local forward tangent model optimized at 6 months starting from March 1982 under the new norm, and (b) its final pattern after a 6-month evolution.

second singular vector may have a larger growth rate than that of the first singular vector because the singular vectors are meant to optimize the ratio of the energy norm of e_j and the new norm of e_{j0} rather than the simple ratio of the energy norm of e_j and e_{j0} .

We found that the first singular vector is not sensitive to initial time and optimization time. A typical first singular vector and its final pattern are shown in Fig. 17. It is seen that the SST and winds grow stationary, while the thermocline depth grows and propagates eastward. The fact that the first singular vector has most of its energy in the first few EOFs (Fig. 18) is not surprising since the new norm has taken account of the initial error covariance, which itself is dominated by the first few EOFs (Fig. 1c). The comparison of Figs. 18 and 7 reveals that the first singular vector under the energy norm

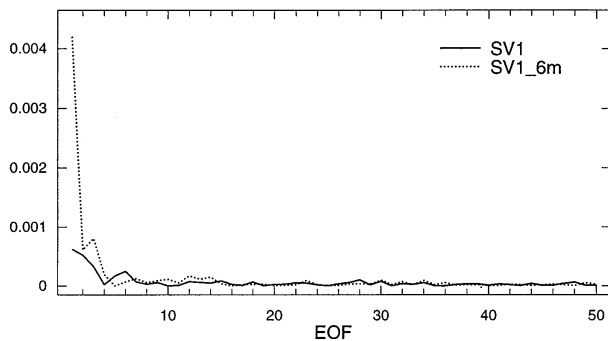


FIG. 18. As in Fig. 7 except the first singular vectors are under the new norm.

is more efficient in drawing energy from the background state than the first singular vector under the new norm.

The set of singular vectors of each forward tangent model spans a complete space into which the old and new ICs can be decomposed. Figure 19 shows that the first singular vector components of the old and new ICs vary in phase with the ENSO cycles. During the warm events, the first singular vector components are positive; during the cold events, they are negative. This is not surprising since the SST and wind fields of the first singular vector mimic a mature phase of ENSO (Fig. 17a). The differences between the first singular vector components of the old and new ICs are also the first singular vector components of the error fields of the old ICs. It is seen that they are large during the periods when the old and new forecasts differ significantly, for example, during the years of 1972, 1976, 1977, 1978, 1981, 1983, 1984, 1985, 1987, 1989, 1990, and 1994 (Figs. 1a, 1b, and 19). The size of the first singular vector components of the initial error fields is at times 10 times that shown in Fig. 17a. These errors are certainly much larger than the observational errors.

The first singular vector components are the most important components of the initial errors because of their fast growth rate. If the first singular vector components of the initial errors are removed from the old ICs, we found that the forecast skill verified at the period between January 1972 and December 1992 is significantly improved (Fig. 20). When all of the 50 singular vector components of the initial errors are removed from the old ICs, the skill of the new forecasts is recovered

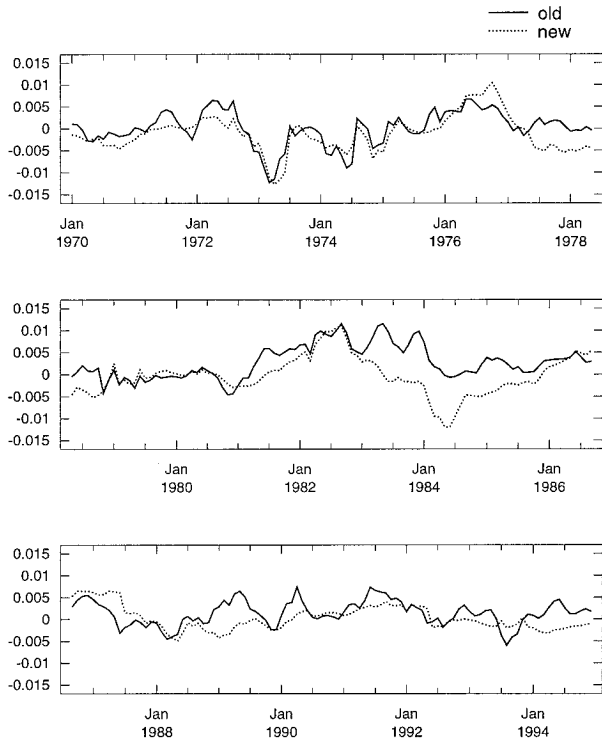


FIG. 19. The amplitudes of the first singular vector components of the old (solid line) and new (dotted line) initial conditions. The first singular vectors are those of the local forward tangent models for the old initial conditions optimized at 6 months under the new norm.

within 1-yr lead time. However, at longer lead times the skill is apparently sensitive to the EOFs higher than the 50th. When the old ICs are corrected with the first singular vector components, the forecast skill at all lead times between 2 and 9 months is significantly better than that of the old forecasts and is comparable to that of the new forecasts. The results indicate that essentially one initial error structure is responsible for most of the improvement of the forecast skill of the new forecasts.

Although the singular vectors are orthogonal in the multivariate EOF space, the single variable fields of the singular vectors are not orthogonal. The variance percentage of a single variable accounted for by the first singular vector component is calculated by

$$\mu = 1 - \frac{\|\mathbf{z} - \mathbf{z}'\|^2}{\|\mathbf{z}\|^2}, \quad (6)$$

where \mathbf{z} is the original variable vector and \mathbf{z}' is the variable vector described by the first singular vector component. When μ is close to 1, the variable is adequately represented by the first singular vector component; when μ is less than zero, the error variance is larger than the signal variance, so the variable is poorly represented. We are concerned with how well the oceanic variables, SST, and winds of the initial errors are represented by the first singular vector components. The

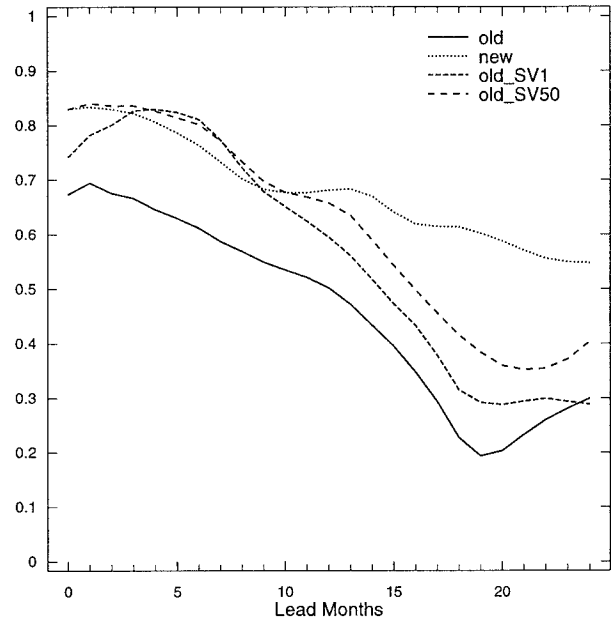


FIG. 20. Correlation between the observed Nino-3 verified between January 1972 and December 1992, and the model-simulated Nino-3 starting from the old initial conditions (solid line), from the new initial conditions (dotted line), from the corrected old initial conditions with the first singular vector components of the difference fields between the new and old initial conditions (short-dashed line), and from the corrected old initial conditions with all of the 50 singular vector components of the difference fields (long-dashed line).

variance of the oceanic variables is defined as the sum of the variance of thermocline depth, zonal, and meridional currents. Figure 21 shows that the SST and wind errors are generally better represented than the oceanic variables are. It is noticed that a large singular vector component of the initial errors is usually associated with a large variance percentage of the SST and wind errors (Figs. 19 and 21). January 1984 is an exception where the variance percentage of the SST and wind errors is less than zero, while the singular vector component of the initial errors is quite large. But the oceanic variables of the initial errors are well represented (50%). Another period where the oceanic variables of the initial errors are well represented by the singular vector component is fall 1977. When the first singular vector components are used to correct the old ICs, no matter whether the SST and wind errors or the oceanic variable errors are corrected, the forecasts are improved significantly over the old forecasts. The results suggest that, overall, the correction of the initial SST and wind errors is more critical to the improvement of forecasts than the correction of the oceanic variable errors. The periods around fall 1977 and January 1984 are special where the correction of the oceanic variable errors may be as important as the correction of the SST and wind errors.

7. Summary and discussions

The predictability of ENSO is addressed by applying singular vector analysis to the ENSO forecast model of

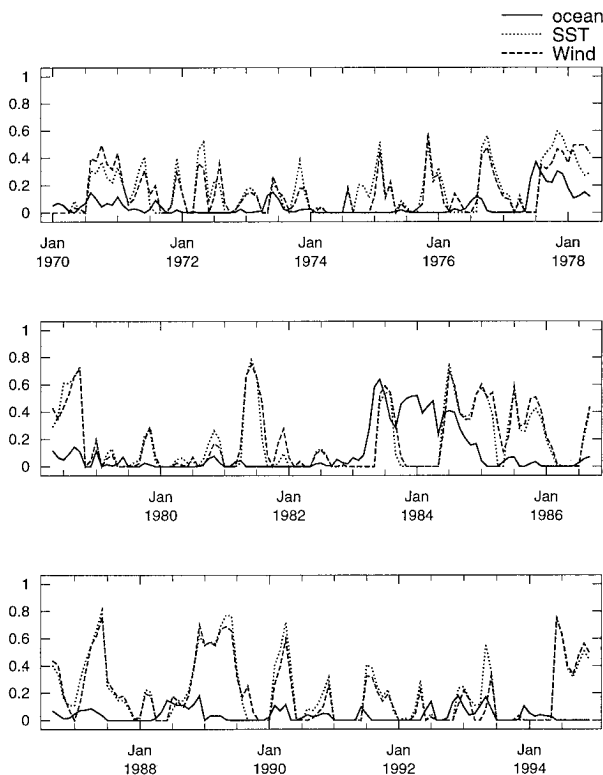


FIG. 21. The variance percentage of the oceanic variables (solid line), SST (dotted line), and wind (dashed line) fields of the initial errors accounted for by the first singular vector components. When it is less than zero, which means that the field is poorly represented, it is plotted zero here for clarity.

Zebiak and Cane (1987). In Part I (Xue et al. 1997) we explored the optimal growth of the seasonal background (zero anomaly) and the ENSO cycles in a long model run. Under the energy norm, one dominant singular vector is found, which varies little with initial time and optimization time. The optimal growth rate, as measured by the largest singular value, is seasonal and attributable to the seasonal background. For a 6-month optimization, the early spring start has the largest growth rate because the SST anomalies in the eastern Pacific produce maximum wind responses in spring when the ITCZ is closest to the equator, and the subsequent growth in summer is large because of the large mean SST gradient and strong mean upwelling (Tziperman et al. 1997); the fall start has the smallest growth rate since the growth seasons of spring and summer are excluded.

Here this singular vector analysis tool was applied to the actual ENSO cycles in the ZC forecasts. The two sets of forecasts using the standard and new initialization procedures (Chen et al. 1995) were analyzed. The forecasts using the new initialization are significantly better than those using the standard initialization (Chen et al. 1995). The purpose of the singular vector analysis is to study the initial error growth in the two sets of

forecasts and to understand the limits of the present ZC forecast system.

One dominant singular vector, similar to that in Part I, is found. Most of the variation in the optimal growth rate is seasonal and attributable to the seasonal variation in the background states. However, the seasonal growth rate is occasionally either suppressed or enhanced by the interannually varying ENSO states. Generally speaking, the cold events are more stable than the warm events. Starting from similar first singular vector perturbations, the final patterns of the perturbations are found to be confined to the eastern Pacific during the warm events, but they spread to both the western and eastern Pacific during the cold events and mean condition. These are related to the different thermodynamics of the cold and warm events (see Part I). The energy distribution of the first singular vector is quite white in the EOF space, but the final pattern is dominated by the first EOF. The energy norm amplifies from 5- to 24-fold in 6 months. This indicates that small-scale disturbances are able to draw energy efficiently from the mean seasonal background states and evolve into large scales, characteristic of ENSO, in several months. This phenomenon is similar to that in numerical weather prediction, within which subsynoptic-scale disturbances are critical to the development of synoptic-scale circulations.

The comparison of the optimal growth of the old and new forecasts reveals significant differences during the periods when the two sets of forecasts are different. When the control run trajectories of 6-month forecasts are in different dynamic regimes, the optimal growth is expected to be different. In such situations, singular vector analysis is not a valid tool to address the predictability of ENSO because the local linear growth rate need not correspond to the true nonlinear growth rate. When the optimal growths of the two forecasts are consistent, they agree well with that due to the seasonal background alone, except they are much smaller in cold phases. Therefore the predictability is seasonal to first order.

The main constraint on the forecast skill with the standard initialization is due to the large initial errors, rather than the inherent linear predictability. If the difference fields between the old and new ICs are considered as the error fields of the old ICs, they are often larger than the observational errors. However, in a few cases, such as during the spring of 1972 and the year of 1981, the local growth rate is so large that predictability appears to be a major factor limiting forecast skill. Moreover, the false ENSO alarms that the model made in the past two decades with the standard initialization are believed to be associated with the large growth rate of the system (Fig. 6).

Optimal growth represents dominant initial error growth only when initial error covariance is white under a choice of norm. Under the energy norm the error fields of the old ICs are not white but are dominated by the

first few EOFs. A new norm is defined as the inner product weighted by the inverse of the initial error covariance so that the initial error covariance under the new norm is the identity matrix. The singular vectors and singular values, maximizing the ratio of the energy norm of final perturbations and the new norm of initial perturbations, were calculated. One dominant singular vector was found; it is not sensitive to initial time and optimization time. This singular vector contains mostly low EOF components. The growth rate of the first singular vector, measured by the ratio of the energy norm of final and initial perturbations, is much smaller than the optimal growth rate under the energy norm discussed earlier; however, the variability of this growth rate as a function of initial states is qualitatively similar to that of the optimal growth rate.

The first singular vector components of the error fields of the old ICs vary with initial times and have amplitudes that are often much larger than the observation errors. If the first singular vector components of the initial errors are removed from the old ICs, the forecast skill is improved significantly, recovering most of the forecast skill of the new forecasts at lead times of 1 year or less. The result indicates that this one error structure is largely responsible for most of the improvement of the forecast skill. Even though the initial errors are sometimes so large that they evolve in the nonlinear regime, the linear singular vector analysis under a norm defined by the initial error covariance is useful in selecting the major and fastest-growing components of the initial errors. In contrast, the dominant singular vector under the energy norm does not describe the initial errors well. This result supports the argument of Palmer (1996) that the norm for singular vector analysis should be chosen in such a way that the initial error PDF is isotropic.

The old forecasts are impaired by the initial error fields, which vary with initial states and evolve nonlinearly. The new initialization procedure, in which the forced simulations are reconciled with the coupled simulations, seems to be effective in reducing the large-scale imbalances between the model and data in the old ICs to reduce the initialization shock. Also the new initialization better balances using observations and minimizing the optimal growth of the system, which probably contributes to the improvement of the new forecasts significantly. Further progress in initialization procedures is likely to yield further improvements in forecast skill. In the future, with a better knowledge of

the initial error PDF, ensemble forecasts with dominant singular vectors as perturbations are expected to improve ENSO forecast skill as well.

Acknowledgments. This research has been supported by the TOGA Program on Seasonal to Interannual Prediction through National Oceanic and Atmospheric Administration Grant NA16RC0432-03. We appreciate the very thoughtful comments of the anonymous reviewers.

REFERENCES

- Buizza, R., and T. N. Palmer, 1995: The singular-vector structure of the atmospheric global circulation. *J. Atmos. Sci.*, **52**, 1434–1456.
- Cane, M. A., S. E. Zebiak, and S. C. Dolan, 1986: Experimental forecasts of El Niño. *Nature*, **321**, 827–832.
- Chen, D., S. E. Zebiak, A. J. Busalacchi, and M. A. Cane, 1995: An improved procedure for El Niño forecasting. *Science*, **269**, 1699–1702.
- Chen, Y.-Q., D. S. Battisti, T. N. Palmer, J. Barsugli, and E. S. Sarachik, 1997: A study of the predictability of tropical Pacific SST in a coupled atmosphere–ocean model using singular vector analysis: The role of the annual cycle and the ENSO cycle. *Mon. Wea. Rev.*, **125**, 831–845.
- Latif, M., T. P. Barnett, M. A. Cane, M. Flügel, N. E. Graham, H. von Storch, J.-S. Xu, and S. E. Zebiak, 1994: A review of ENSO prediction studies. *Climate Dyn.*, **9**, 167–179.
- Lorenz, E. N., 1965: A study of the predictability of a 28-variable atmospheric model. *Tellus*, **3**, 321–333.
- Molteni, F., and T. N. Palmer, 1993: Predictability and finite-time instability of the northern winter circulation. *Quart. J. Roy. Meteor. Soc.*, **119**, 269–298.
- , R. Buizza, T. N. Palmer, and T. Petroliaigi, 1996: The ECMWF ensemble prediction system: Methodology and validation. *Quart. J. Roy. Meteor. Soc.*, **122**, 73–119.
- Moore, A. M., and R. Kleeman, 1996: The dynamics of error growth and predictability in a coupled model of ENSO. *Quart. J. Roy. Meteor. Soc.*, **122**, 1405–1446.
- Palmer, T. N., 1996: Predictability of the atmosphere and oceans: From days and decades. *Decadal Climate Variability: Dynamics and Predictability*, D. Anderson and J. Willebrand, Eds., Springer, 83–155.
- , and D. L. T. Anderson, 1994: The prospects for seasonal forecasting—A review paper. *Quart. J. Roy. Meteor. Soc.*, **120**, 755–793.
- Tziperman, E., S. E. Zebiak, and M. A. Cane, 1997: Mechanisms of seasonal–ENSO interaction. *J. Atmos. Sci.*, **54**, 61–71.
- Xue, Y., M. A. Cane, S. E. Zebiak, and B. Blumenthal, 1994: On the prediction of ENSO: A study with a low-order Markov model. *Tellus*, **46A**, 512–528.
- , —, and —, 1997: Predictability of a coupled model of ENSO using singular vector analysis. Part I: Optimal growth in seasonal background and ENSO cycles. *Mon. Wea. Rev.*, **125**, 2043–2056.
- Zebiak, S. E., and M. A. Cane, 1987: A model El Niño–Southern Oscillation. *Mon. Wea. Rev.*, **115**, 2262–2278.